JOURNAL OF GUIDANCE, CONTROL, AND DYNAMICS
Vol. 19, No. 6, November–December 1996

Spacecraft Attitude Estimation Using the Global Positioning System: Methodology and Results for RADCAL

Penina Axelrad* and Lisa M. Ward†
University of Colorado, Boulder, Colorado 80309

Methodology and results for the Global Positioning System based attitude determination of a gravity gradient stabilized satellite are presented. Algorithms for on-orbit antenna baseline estimation, attitude initialization, point solution, and Kalman filtering are described. These algorithms are demonstrated using flight data collected on board the U.S. Air Force RADCAL Satellite. The precision of the final attitude estimates is assessed to be at the level of 0.4 deg for pitch and roll and 0.7 deg for yaw.

Nomenclature

B	= body frame
$\boldsymbol{b}$	= baseline vector
$\boldsymbol{C}$	= transformation matrix from orbit local to body frame
$\boldsymbol{e}$	= line of sight unit vector
$\boldsymbol{H}$	= measurement gradient matrix
$\boldsymbol{I}$	= identity matrix
I_1, I_2, I_3	= principal moments of inertia
i_A, j_A, k_A	= basis vectors for coordinate frame A
k	= integer cycle
L	= orbit local frame
$\boldsymbol{q}$	= four-element attitude quaternion from orbit local to body frame
$\boldsymbol{V}^{\times}$	= cross product matrix associated with the vector $\boldsymbol{v}$; $\boldsymbol{V}^{\times} = \begin{bmatrix} 0 & v_3 & -v_2 \\ -v_3 & 0 & v_1 \\ v_2 & -v_1 & 0 \end{bmatrix}$
$\boldsymbol{x}$	= state vector
$\boldsymbol{z}$	= measurement residual vector
β	= line bias
Δr	= range difference
$\Delta\varphi$	= measured phase difference
$\delta\boldsymbol{q}$	= three-element correction quaternion
$\delta\varphi$	= phase difference residual
$\delta(\cdot)$	= estimation error of a given quantity
v	= phase difference measurement error
Ω	= spacecraft orbital rate
ω	= inertial angular velocity of the body in body coordinates
ω_L	= local angular velocity of the body
$(\cdot)^A$	= vector quantity expressed in coordinate frame A
$\hat{(\cdot)}$	= estimate of a quantity
$\otimes$	= quaternion composition operation; see Ref. 1

I. Introduction

THE Global Positioning System (GPS), comprising a constellation of 24 satellites and a ground monitoring and control network, is widely used for positioning of vehicles near the surface of the Earth and for orbit determination of near-Earth satellites. In addition to these functions, GPS is capable of providing vehicle attitude through the use of L-band carrier phase interferometry between multiple antennas. This technique is of particular interest for near-Earth space applications because of the potential for reducing the number of onboard navigation and attitude sensors and increasing spacecraft autonomy.

GPS-based attitude determination is being considered for a broad range of space platforms from low-cost mobile communications satellites to the Space Station Alpha. Thus far, there have been relatively few flight tests of such a system, namely, the U.S. Air Force RADCAL satellite, NASA GADACS, and the recent launch of REX II. All of these missions have carried a version of the Trimble Navigation TANS Quadrex or Vector receiver, modified by Stanford University for use on orbit.

Attitude determination for satellites has been extensively studied.[1–5] In particular, Lefferts et al.[2] provide a detailed description of a quaternion-based Kalman filter that uses star tracker and gyro measurements. References 6 and 7 describe similar algorithms for integrating GPS with gyro data. A Kalman filter designed specifically for a gravity gradient satellite with various sensors was developed by Melvin.[8]

The first analysis of using satellite radio signals for attitude determination was given by Albertine in 1974 (Ref. 9). The topic went relatively unnoticed until the late 1980s because the size and cost of high-performance GPS equipment made it unrealistic to use multiple receivers or channels to track several antennas on a single vehicle. This changed dramatically with the advent of largely digital receivers. In the next few years a variety of solution algorithms using a single set of simultaneous measurements were proposed.[10–13] These methods, referred to as attitude point solution algorithms, were generally designed for applications on land vehicles, ships, and aircraft.

In the early 1990s, C. E. Cohen together with Trimble Navigation developed a receiver architecture and algorithms for attitude determination.[14,15] In his doctoral dissertation and other references,[15,16] Cohen described a variety of algorithms for attitude point solutions, initialization, and ambiguity resolution. Some of these are implemented in the TANS vector receiver to provide real-time attitude point solutions.

The first space flight experiment of GPS for attitude estimation was the U.S. Air Force RADCAL satellite. Lightsey et al.[17] described the use of GPS on board such a vehicle and evaluated the likely error sources. References 18 and 19 described the preliminary results they generated from actual RADCAL data. They analyzed a single 4-h section of data from RADCAL and produced orbit estimates and attitude point solutions. They noted that the accuracy of the solutions is limited by the absence of reliable baseline estimates and measurement errors, which are likely to be dominated by multipath.

This paper extends the theoretical work of Cohen et al.[15–19] in using GPS alone for spacecraft attitude estimation and presents more comprehensive experimental results. We provide a systematic approach to attitude estimation from initialization to filter refinement with algorithm enhancements at each step. The initialization routine and point solution algorithms are reformulated in terms of

Received Oct. 31, 1994; revision received April 18, 1996; accepted for publication May 2, 1996.

*Assistant Professor, Department of Aerospace Engineering Sciences, Colorado Center for Astrodynamics Research, Campus Box 431. Member AIAA.

†Graduate Student, Department of Aerospace Engineering Sciences. Member AIAA.

quaternions rather than Euler angles. The attitude estimator is implemented as an extended Kalman filter also in terms of quaternions, making it more tolerant of large-amplitude oscillations in pitch and roll and an unconstrained yaw rate. A baseline filter is developed that uses flight data to refine the estimates of the relative locations of the antennas, thereby reducing a significant source of error in earlier results.[18,19] Furthermore, the various algorithms are rigorously applied to many data sets available for RADCAL, amounting to over 50 h of solutions. Because of the lack of an external attitude reference on RADCAL, accuracy is assessed by numerous consistency checks between various solution methods.

The remainder of this paper is organized as follows. Section II develops the basic GPS phase difference observable. Section III presents each of the steps in the final attitude estimation process including initialization, attitude and baseline filters, and the point solution algorithm. Section IV describes the flight data and discusses the results obtained. Finally, Sec. V summarizes the paper and presents some ideas for future research.

II. Attitude and the GPS Phase Difference Observable

The attitude of a spacecraft is its orientation with respect to some frame of reference. More specifically for this study, it is the rotation of a coordinate frame fixed in the spacecraft body, with respect to the orbit local frame. The orbit local frame L is centered on the spacecraft and aligned with the radial and orbit normal vectors, as shown in Fig. 1. The body-fixed frame B is aligned with the principal axes of the spacecraft. The rotation from the local to the body frame can be represented by a transformation matrix C. It can also be represented by a four-element attitude quaternion $\boldsymbol{q}$.

Most attitude sensors, such as sun sensors or magnetometers, are based on the principle of measuring a vector in both the body frame and the reference frame and then determining the rotation between the two frames (see, for example, Ref. 8). A similar approach is taken when using GPS-based measurements. Cohen[15] formulated the attitude determination problem in terms of the GPS observable. In this section we summarize his results to aid in our discussion.

All GPS satellites generate a carrier signal at the L1 frequency. This frequency is centered on 1575.42 MHz, which corresponds to a wavelength of 19.03 cm. The fractional difference in carrier phase between two antennas, $\Delta\varphi$, forms the principal observable for attitude determination using GPS. One antenna is designated as the master antenna, and the others are slaves. This phase difference can be expressed by

$$\Delta\varphi = \Delta r - k + \beta + \nu \tag{1}$$

The range difference Δr is given by

$$\Delta r = r_m - r_s \tag{2}$$

where r_m is the distance from the master to a GPS satellite and r_s is the distance from the slave to the same satellite expressed in L1 cycles. The term k is the integer number of carrier cycles in the range difference. The hardware line bias β is the difference in delays produced by cables and electronics between the master and slave antenna expressed in fractional cycles. The term ν is the random measurement noise, also expressed in cycles.

As illustrated in Fig. 2, the range difference is the projection of the baseline vector $\boldsymbol{b}$ (directed from master to slave) onto the line of sight vector $\boldsymbol{e}$, which gives

$$\Delta r = \boldsymbol{b} \cdot \boldsymbol{e} = |\boldsymbol{b}| \cos\theta \tag{3}$$

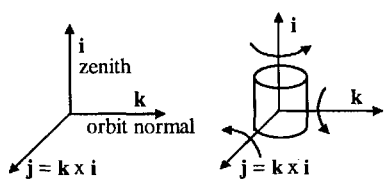

Fig. 1 Reference frames.

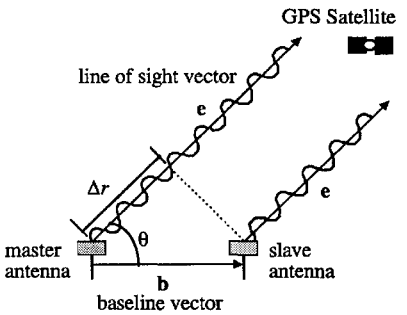

Fig. 2 GPS phase difference geometry.

If $\boldsymbol{e}$ is expressed in the orbit local reference frame and $\boldsymbol{b}$ is known in the body-fixed reference frame, the range difference may be written as

$$\Delta r = (\boldsymbol{b}^B)^T \boldsymbol{C}\boldsymbol{e}^L \tag{4}$$

and the observed phase difference is given by

$$\Delta\varphi = (\boldsymbol{b}^B)^T (\boldsymbol{C}\boldsymbol{e}^L) - k + \beta + \nu \tag{5}$$

Given a minimum number of observations, for example, three baselines observing two satellites, the attitude can be solved deterministically. If more measurements are available, the solution can be optimized in some way. Generally, the attitude matrix is not solved for explicitly. Instead, it is modeled by a linear correction to an a priori estimate, $\hat{\boldsymbol{C}}$. We assume that the a priori estimate of the attitude matrix is related to the true attitude according to

$$\boldsymbol{C} = \delta\boldsymbol{C}\hat{\boldsymbol{C}} \equiv (\boldsymbol{I} + \boldsymbol{Q}^{\times})\hat{\boldsymbol{C}} \tag{6}$$

where the transformation matrix $\delta\boldsymbol{C}$ is expressed in terms of a small correction quaternion $\delta\boldsymbol{q}$ and $\boldsymbol{Q}^{\times}$ is the cross product matrix associated with the elements of the vector $\delta\boldsymbol{q}$.

The observed phase for baseline i and satellite j can then be related to the quaternion correction by substituting Eq. (6) into Eq. (5) and expanding:

$$\Delta\varphi_{ij} = \left(\boldsymbol{b}_i^B\right)^T \left(\hat{\boldsymbol{C}}\boldsymbol{e}_j^L\right) + \left(\boldsymbol{b}_i^B\right)^T \left(2\boldsymbol{Q}^{\times}\hat{\boldsymbol{C}}\boldsymbol{e}_j^L\right) - k_{ij} + \beta_i + \nu_{ij} \tag{7}$$

The second term in Eq. (7) can be rearranged as follows:

$$\left(\boldsymbol{b}_i^B\right)^T \left(2\boldsymbol{Q}^{\times}\hat{\boldsymbol{C}}\boldsymbol{e}_j^L\right) = 2\left(\hat{\boldsymbol{C}}\boldsymbol{e}_j^L\right)^T \boldsymbol{B}_i^{\times}\delta\boldsymbol{q} \tag{8}$$

where $\boldsymbol{B}_i^{\times}$ is the cross product matrix associated with the components of the vector $\boldsymbol{b}_i^B$. If the integer and line bias are known, the predicted phase is given by

$$\Delta\hat{\varphi}_{ij} = \left(\boldsymbol{b}_i^B\right)^T \left(\hat{\boldsymbol{C}}\boldsymbol{e}_j^L\right) - k_{ij} + \beta_i \tag{9}$$

The phase difference residual $\delta\varphi_{ij}$ is given by

$$\delta\varphi_{ij} \equiv \Delta\varphi_{ij} - \Delta\hat{\varphi}_{ij} \tag{10}$$

where $\Delta\varphi_{ij}$ is the observed phase difference measurement and $\Delta\hat{\varphi}_{ij}$ is the predicted phase difference measurement. We can model this residual as

$$\delta\varphi_{ij} = 2\left(\hat{\boldsymbol{C}}\boldsymbol{e}_j^L\right)^T \boldsymbol{B}_i^{\times}\delta\boldsymbol{q} \tag{11}$$

if we assume the measurement errors ν_{ij} have zero mean. This equation can then be used to solve for $\delta\boldsymbol{q}$.

III. Methodology

This paper describes a sequence of algorithms, which begin with the most basic assumptions about the vehicle attitude and ultimately

produce high-accuracy attitude solutions based on GPS measurements. We begin with an attitude initialization step followed by an extended Kalman filter for attitude and line biases, with the option of refining the baseline estimates using data collected on orbit. A point solution algorithm is also used for comparison purposes. An overview of the process is given next, followed by a detailed description of each algorithm.

Initially we assume that the baselines, line biases, integer ambiguities, and attitude of a spacecraft are unknown. To begin the attitude estimation process, rough estimates of both vehicle attitude and antenna locations are needed. Broad assumptions can be made about the attitude of a spacecraft based on vehicle design and/or GPS satellite visibility. For example, a gravity gradient satellite would most likely be nadir pointing. Checking received GPS signal strength could verify this assumption and provide additional attitude information. Cohen[15] developed a ground-based static self-survey algorithm to determine the antenna baselines in the spacecraft body frame to an accuracy of several millimeters. Without the self-survey, however, one must rely on mechanical drawings of the spacecraft, which should provide the antenna baselines to within several centimeters. The ad hoc attitude and baseline estimates described earlier are sufficient to start the attitude estimation process.

Since the receiver only measures the fractional part of the phase difference, the range difference remains ambiguous until the integer part is resolved. Both the point solution and the Kalman filter require that the attitude, angular velocity, and line biases are known to an equivalent uncertainty of one-quarter of a wavelength so that the integers can be resolved directly. The one-quarter wavelength constraint comes from the fact that if the combined errors are larger than one-half wavelength, an incorrect integer could result as a result of rounding; therefore, a conservative constraint of one-quarter wavelength is chosen to ensure that the proper integer is calculated. To meet this requirement, the initialization algorithm is employed to improve the a priori estimate of the attitude to within 10 deg. With accurate baselines, enough information is now available to apply the attitude Kalman filter and to obtain accurate results. However, if the baselines are not well known, the baseline estimator may be used to improve the knowledge of the relative antenna coordinates and the line biases before running the attitude filter. Table 1 lists the input requirements and expected performance of each algorithm.

Attitude Point Solution

The attitude point solution is an iterative least-squares fit to a set of simultaneous observations. Since no dynamic models of the system are incorporated into the solution, the point estimates are noisy. However, they serve as a benchmark against which other methods can be compared.

The approach we use is to solve for the state vector,

$$\boldsymbol{x} = [\delta q_1 \quad \delta q_2 \quad \delta q_3]^T \tag{12}$$

using the following equation to predict the phase difference:

$$\Delta\hat{\varphi}_{ij} = \left(\boldsymbol{b}_i^B\right)^T \left(\hat{\boldsymbol{C}}\boldsymbol{e}_j^L\right) + \beta_i - \hat{k}_{ij} \tag{13}$$

Table 1 Algorithm requirements and performance

Algorithm	Parameter	Input requirements	Output performance
Attitude initialization	Attitude	Very coarse	10 deg
	Baselines	2 cm	N/A
	Line biases	——	$\frac{1}{4}$ cycle
Attitude filter	Attitude	10 deg	0.2 deg
	Baselines	5 mm	N/A
	Line biases	$\frac{1}{4}$ cycle	0.03 cycles
Baseline estimator	Attitude	10 deg	N/A
	Baselines	2 cm	5 mm
	Line biases	$\frac{1}{4}$ cycle	0.03 cycles
Point solution	Attitude	10 deg	1.0 deg
	Baselines	5 mm	N/A
	Line biases	$\frac{1}{4}$ cycle	N/A

In this formulation the line bias is assumed to be known, and the integer $\hat{k}_{ij}$ is calculated as follows:

$$\hat{k}_{ij} = \text{int}\left[\left(\boldsymbol{b}_i^B\right)^T \left(\hat{\boldsymbol{C}}\boldsymbol{e}_j^L\right) + \beta_i - \Delta\varphi_{ij}\right] \tag{14}$$

where the int function rounds to the nearest integer. We assume that $\hat{k}_{ij}$ is always correct because the a priori attitude is always good enough to resolve it. However, if there are large gaps in the data, this assumption may not be true, which could result in an incorrect solution.

The measurement gradient, $\boldsymbol{H}_{ij} = \partial(\Delta\varphi_{ij})/\partial\boldsymbol{x}$, is given by

$$\boldsymbol{H}_{ij} = 2\left(\hat{\boldsymbol{C}}\boldsymbol{e}_j^L\right)^T \boldsymbol{B}_i^{\times} \tag{15}$$

for a single observation on baseline i and satellite j. The measurement gradient vectors for all of the observations at a particular measurement epoch are concatenated into an $m \times n$ matrix $\boldsymbol{H}$, where m is the number of measurements at the epoch and n is the number of states. The measurement residuals are then combined into an m-vector z to give

$$z = \begin{bmatrix} \vdots \\ \Delta\varphi_{ij} - \Delta\hat{\varphi}_{ij} \\ \vdots \end{bmatrix} \tag{16}$$

At each measurement epoch we solve the system of equations $\boldsymbol{H}\hat{\boldsymbol{x}} = z$ for $\hat{\boldsymbol{x}}$ to find the best estimate of the correction quaternion $\delta\hat{\boldsymbol{q}}$. The full correction quaternion is formed using the equation

$$\delta\hat{\boldsymbol{q}} = \begin{bmatrix} \delta\hat{\boldsymbol{q}} \\ \sqrt{1 - \delta\hat{q}_1^2 - \delta\hat{q}_2^2 - \delta\hat{q}_3^2} \end{bmatrix} \tag{17}$$

Then the updated quaternion estimate $\hat{\boldsymbol{q}}^+$ is computed by composing the full correction quaternion with the a priori estimate, $\hat{\boldsymbol{q}}^-$, as follows:

$$\hat{\boldsymbol{q}}^+ = \delta\hat{\boldsymbol{q}} \otimes \hat{\boldsymbol{q}}^- \tag{18}$$

The process is repeated until $\delta\hat{\boldsymbol{q}}$ gets sufficiently small.

Note that line biases are not estimated in this implementation. However, if the line biases are not well known or are fluctuating as a result of thermal variations, they could easily be added to the state vector. Adding the line biases would reduce the errors introduced by an incorrect a priori estimate of the line bias but may increase the sensitivity of the solution to multipath errors.

Attitude Initialization Algorithm

The batch process presented here is a method of estimating the initial attitude, angular velocity, and integer ambiguities for a spacecraft. These values can then be used as starting points for the other attitude estimation algorithms. This algorithm is based on the method described by Cohen and Parkinson.[20] Our implementation includes guidelines for selecting data and a robust solution consistency check.

The vehicle is assumed to rotate with constant angular velocity so that the attitude matrix can be represented as

$$\boldsymbol{C} = \boldsymbol{C}\left(\omega_L^B t\right)\boldsymbol{C}(\boldsymbol{q}_0) \tag{19}$$

where the quaternion $\boldsymbol{q}_0$ represents the attitude of the vehicle with respect to the local frame at some initial time t_0 and ω_L^B is the (assumed) constant angular velocity vector of the vehicle with respect to the local frame expressed in body coordinates. With an a priori initial attitude $\hat{\boldsymbol{q}}_0$ and angular velocity $\hat{\omega}_L^B$, we can model $\boldsymbol{C}$ using the following equation:

$$\boldsymbol{C} = \delta\boldsymbol{C}\hat{\boldsymbol{C}} \equiv \left(\boldsymbol{I} + \Theta^{\times}\right)\boldsymbol{C}\left(\hat{\omega}_L^B t\right)\boldsymbol{C}(\hat{\boldsymbol{q}}_0) \tag{20}$$

where t is the time since t_0. The vector $\boldsymbol{\theta}$ represents small rotations about the initial estimate of the body axes and is given by

$$\boldsymbol{\theta} = 2\delta\boldsymbol{q} + \delta\omega_L^B t \tag{21}$$

and $\Theta^{\times}$ is the cross product matrix associated with the components of $\boldsymbol{\theta}$.

The state vector is defined as

$$\boldsymbol{x} = \left[\delta q_1 \quad \delta q_2 \quad \delta q_3 \,\middle|\, \delta\omega_{L1}^B \quad \delta\omega_{L2}^B \quad \delta\omega_{L3}^B \,\middle|\, \kappa_{11} \quad \cdots \quad \kappa_{mn}\right]^T \tag{22}$$

where

$$\kappa_{ij} = k_{ij} - \beta_{ij} \tag{23}$$

that is, κ_{ij} is a floating point number that includes both the integer cycle and the line bias. This leads to the following model for the observed phase difference:

$$\Delta\varphi_{ij} = \left(\boldsymbol{b}_i^B\right)^T\left(\hat{\boldsymbol{C}}\boldsymbol{e}_j^L\right) + \left(\boldsymbol{b}_i^B\right)^T\left(\Theta^{\times}\hat{\boldsymbol{C}}\boldsymbol{e}_j^L\right) - \hat{\kappa}_{ij} + \nu \tag{24}$$

Now the predicted phase difference for baseline i and satellite j is

$$\Delta\hat{\varphi}_{ij} = \left(\boldsymbol{b}_i^B\right)^T\left(\hat{\boldsymbol{C}}\boldsymbol{e}_i^L\right) \tag{25}$$

The measurement gradient H_{ij} for a single measurement is given by

$$\boldsymbol{H}_{ij} = \left[2\left(\hat{\boldsymbol{C}}\boldsymbol{e}_j^L\right)^T B_i^{\times} \,\middle|\, \left(\hat{\boldsymbol{C}}\boldsymbol{e}_j^L\right)^T B_i^{\times} t \,\middle|\, 0 \quad \cdots \quad 0 \quad -1 \quad 0 \quad \cdots \quad 0\right] \tag{26}$$

The measurement gradient vectors for the entire batch of observations are concatenated into an $m \times n$ matrix $\boldsymbol{H}$, where m is the number of measurements in the batch and n is the number of states. The measurement residuals, calculated according to Eq. (16), are then combined into a m-vector $\boldsymbol{z}$.

Now, to find the best estimate of the corrections, we solve the system of equations $\boldsymbol{H}\hat{\boldsymbol{x}} = \boldsymbol{z}$ for $\hat{\boldsymbol{x}}$. The quaternion corrections are converted to a full quaternion as in Eq. (17), which is then used to update the a priori estimate of $\boldsymbol{q}_0$ according to the quaternion composition rule. The angular velocity is updated in the traditional manner by adding the correction to the a priori estimate. This batch process is iterated until the corrections become sufficiently small.

At this point there are two checks to determine whether the algorithm has provided the correct answer. The first check is to determine whether the process has converged to a solution. The second check is to determine whether the converged solution is correct. If the process does not converge within a few iterations, 10 at most, this indicates that the initial conditions were not close enough to the solution. Another set of initial conditions is chosen, and the procedure is repeated. For a gravity gradient stabilized satellite like RADCAL, the pitch and roll angles are usually known to within 20 deg. The yaw angle, however, is completely unknown. In this situation, choosing four sets of initial conditions with the yaw angles separated by 90 deg produced at least one convergent answer.

The validity of the solution is verified using the fractional part of each κ_{ij}, which represents the differential line bias between the two antennas. We can estimate the line bias associated with a baseline i by averaging over all satellites $j = 1, \ldots, l$, where l is the number of GPS satellites. Proximity of the fractional portions is used as an integrity check of the algorithm. The largest difference between line bias estimates for a baseline provides a measure of proximity. If the largest difference is at most one-quarter cycle for two out of three baselines, the solution is deemed correct.

Since this algorithm uses very little a priori information, the key to success lies in proper data selection. The following are important factors in the data selection process.

Interval Length

The length of the interval must be long enough to obtain adequate information to resolve the ambiguities but short enough so that the assumption that angular velocity is constant is not violated. We found 10 min of data to be optimal for RADCAL.

Number of GPS Satellites

Since the number of GPS satellites dictates the number of states to be estimated, the number of satellites must be chosen prior to running the algorithm. With too few satellites not enough information will be available to resolve the integers. Too many satellites (and, hence, too many states) could decrease the algorithm's performance. We found that using three or four satellites produced results that passed the check for a correct solution.

Satellite Motion

GPS satellites with large motion relative to the user satellite produce the best results. Large satellite motions produce large changes in the phase difference measurements. Evaluating the change in phase measurement over each baseline for a particular satellite provides a gauge of how much satellite motion is present. Satellites with cycle slips or changes in the master antenna are eliminated. For RADCAL, satellites with a change in phase measurement of less than 0.25 cycle over each baseline are also eliminated. If at least three satellites remain, and the cumulative phase change for the interval is more than eight cycles, then this interval is considered a good candidate. (The cumulative change is calculated by adding the change in phase over each baseline to produce a total change for a satellite, then adding the total change for each satellite to produce a cumulative change for the interval.) In addition to looking for large phase changes, to ensure that the geometry is favorable, we required at least one of the satellites to attain an elevation of 50 deg or more.

Reliable Data

Poor data produced by low signal levels or corrupted by multipath will degrade the performance of this algorithm. To account for this, measurements with a low signal-to-noise ratio (SNR) are filtered out. We found that choosing an SNR cutoff near the median SNR value and filtering out data with SNRs below the cutoff indicated intervals that would yield a correct solution. For the RADCAL data, a cutoff of 6 amplitude measurement units (AMU) was used. (The AMU corresponds to the amplitude of recovered carrier in a bandwidth of 1 kHz.)

If the preceding guidelines for data selection are followed, one should be able to initialize successfully. In some of the flight data sets for RADCAL, however, there were no intervals that satisfied the aforementioned requirements. In those cases, we tried a few intervals of data that did not meet the requirements until one of the intervals produced a consistent solution. With this method we were able to initialize all of the data. Furthermore, each time the line biases were consistent, the solution was in fact within 10 deg of the Kalman filter solution.

Baseline Estimation Algorithm

To properly estimate the attitude of a spacecraft, the body reference frame must be clearly defined, and each of the baselines must be accurately known in this frame. Consider the baseline error Δb shown in Fig. 3. Given this simplified two-dimensional geometry, where $\sin(\Delta\theta) = \Delta b/b$, we can see that a 1-cm baseline error on a 1-m baseline would result in a pointing error of 0.57 deg. For different geometries, the attitude error would vary depending on the orientation of both the baseline and baseline error with respect to the line of sight vector.

If the GPS antennas are not carefully surveyed prior to launch, some assumptions must be made about the relation of the body frame to the antenna array. Mechanical drawings of the spacecraft should provide the location of the antennas to within several centimeters. Refining these estimates is the purpose of the three-step algorithm developed here. First, a sequential filter is used to estimate the line biases, baseline vectors, and local angular velocity. Next,

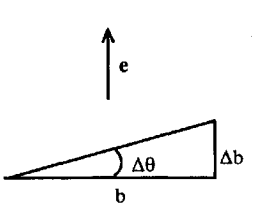

Fig. 3 Effect of baseline error.

the body-fixed frame is defined by two of the local baselines, and all three baselines are transformed from the local frame to the body frame. Finally, the baseline coordinates in the body frame are averaged over time to obtain the best estimate. This method is similar to that presented by Axelrad and Ward.[21]

The 15-element state vector for the sequential filter is given by

$$x = \left[\left(\delta b_1^L\right)^T \ \left(\delta b_2^L\right)^T \ \left(\delta b_3^L\right)^T \,|\, \delta\omega_{L1}^L \ \delta\omega_{L2}^L \ \delta\omega_{L3}^L \,|\, \delta\beta_1 \ \delta\beta_2 \ \delta\beta_3\right]^T \tag{27}$$

where ω_L^L is the angular velocity of the body with respect to the local frame expressed in local coordinates. The phase difference measurement model for baseline i observing satellite j is

$$\Delta\varphi_{ij} = \left(e_j^L\right)^T b_i^L + \beta_i - k_{ij} + \nu \tag{28}$$

or

$$\Delta\varphi_{ij} = \left(e_j^L\right)^T \left(\hat{b}_i^L + \delta b_i^L\right) + \left(\hat{\beta}_i + \delta\beta_i\right) - k_{ij} + \nu \tag{29}$$

and the phase measurement prediction is

$$\Delta\hat{\varphi}_{ij} = \left(e_j^L\right)^T \hat{b}_i^L + \hat{\beta}_i - \hat{k}_{ij} \tag{30}$$

where $\hat{k}_{ij}$ is calculated according to Eq. (14).

Consider a measurement on baseline i observing satellite j. The elements of the measurement gradient matrix for baseline i are the elements of the line of sight vector e_j^L. The element corresponding to the line bias β_i is set to 1. All other elements are zero. For example, if baseline 1 observes satellite j, then

$$H_{1j} = \left[\left(e_j^L\right)^T \ \ 0^T \ \ 0^T \,|\, 0 \ \ 0 \ \ 0 \,|\, 1 \ \ 0 \ \ 0\right] \tag{31}$$

The dynamic model in the filter is given by

$$\frac{db^L}{dt} = \omega_L^L \times b^L \qquad \text{and} \qquad \frac{d\omega_L^L}{dt} = 0 \tag{32}$$

where the derivatives are taken in the local frame.

After the baselines have been estimated in the local frame, the body frame is defined by

$$\hat{j}_B^L \equiv \frac{\hat{b}_2^L}{\left|\hat{b}_2^L\right|}, \qquad \hat{i}_B^L \equiv \frac{\hat{b}_2^L \times \hat{b}_1^L}{\left|\hat{b}_2^L \times \hat{b}_1^L\right|}, \qquad \hat{k}_B^L \equiv \hat{i}_B^L \times \hat{j}_B^L \tag{33}$$

Figure 4 illustrates this definition of the body frame. The estimate of the local to body transformation matrix is constructed at each measurement epoch using the unit vector definitions as follows:

$${}^B\hat{C}^L = \begin{bmatrix} \left(\hat{i}_B^L\right)^T \\ \left(\hat{j}_B^L\right)^T \\ \left(\hat{k}_B^L\right)^T \end{bmatrix} \tag{34}$$

and the estimated local baselines are transformed to the body frame. Since the baseline vectors in the body frame remain constant, their coordinates can be averaged over time to obtain the best estimate.

The baseline estimation process uses the electronic baselines as a basis for the body frame. Generally speaking, all instruments and principal axes can be expressed in a mechanically defined reference frame. To accurately estimate the attitude of the body frame, these two reference frames must be reconciled. Errors in baseline length as well as errors in the direction of one baseline relative to another can be observed with this method. However, a pure rotation between these reference frames will remain transparent (i.e., will appear as an attitude error). A pure rotation can only be resolved by some external means.

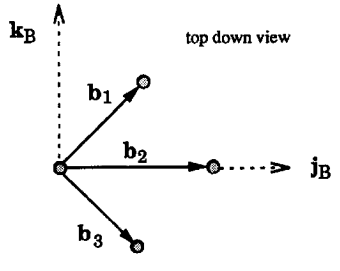

Fig. 4 Definition of the body-fixed frame.

Attitude Kalman Filter

A Kalman filter, by using a dynamical model along with a measurement model, can produce a better solution than the point solution. An extended Kalman filter based on Lefferts et al.[2] is presented next.

The state vector in this formulation is given by

$$x = [\delta q_1 \ \ \delta q_2 \ \ \delta q_3 \,|\, \delta\omega_1 \ \ \delta\omega_2 \ \ \delta\omega_3 \,|\, \delta\beta_1 \ \ \delta\beta_2 \ \ \delta\beta_3]^T \tag{35}$$

where δq, $\delta\omega$, and $\delta\beta$ represent corrections to the local to body quaternion, the inertial angular velocity, and the line biases, respectively. Here the predicted phase difference is given by

$$\Delta\hat{\varphi}_{ij} = \left(b_i^B\right)^T \left(\hat{C}e_j^L\right) + \hat{\beta}_i - \hat{k}_{ij} \tag{36}$$

where $\hat{k}_{ij}$ is calculated according to Eq. (14).

Consider a measurement on baseline i. The element of the measurement gradient matrix corresponding to the line bias β_i is set to 1. The elements for the quaternion states are calculated by the same equation used in the point solution. All other elements are zero. For example, if baseline 1 observes satellite j, then

$$H_{1j} = \left[2\left(\hat{C}e_j^L\right)^T B_1^{\times} \,\middle|\, 0 \ \ 0 \ \ 0 \,\middle|\, 1 \ \ 0 \ \ 0\right] \tag{37}$$

Between measurement epochs, the quaternion and angular velocity states are advanced to the current measurement time by numerically integrating the nonlinear equations of motion for a gravity gradient satellite. These equations, which can be found in Kane et al.,[22] are

$$\begin{aligned} \dot{q}_1 &= \tfrac{1}{2}(\omega_1 q_4 - \omega_2 q_3 + \omega_3 q_2 + \Omega q_2) \\ \dot{q}_2 &= \tfrac{1}{2}(\omega_1 q_3 + \omega_2 q_4 - \omega_3 q_1 - \Omega q_1) \\ \dot{q}_3 &= \tfrac{1}{2}(-\omega_1 q_2 + \omega_2 q_1 + \omega_3 q_4 - \Omega q_4) \\ \dot{q}_4 &= \tfrac{1}{2}(-\omega_1 q_4 - \omega_2 q_2 - \omega_3 q_3 + \Omega q_3) \end{aligned} \tag{38}$$

and

$$\begin{aligned} \dot{\omega}_1 &= K_1\omega_2\omega_3 - 3\Omega^2 K_1 C_{21} C_{31} \\ \dot{\omega}_2 &= K_2\omega_1\omega_3 - 3\Omega^2 K_2 C_{11} C_{31} \\ \dot{\omega}_3 &= K_3\omega_1\omega_2 - 3\Omega^2 K_3 C_{11} C_{21} \end{aligned} \tag{39}$$

where

$$K_1 = \frac{I_2 - I_3}{I_1} \qquad K_2 = \frac{I_3 - I_1}{I_2} \qquad K_3 = \frac{I_1 - I_2}{I_3} \tag{40}$$

The line biases are assumed to be constant. The covariance matrix is propagated forward with the state transition matrix derived from the linearized equations of motion, which are given by

$$\delta\dot{q} = \omega^{\times}\delta q + \tfrac{1}{2}\delta\omega \tag{41}$$

and

$$\begin{aligned} \delta\dot{\omega}_1 &= K_1 6\Omega^2\left[\left(C_{21}^2 - C_{31}^2\right)\delta q_1 - C_{11}C_{21}\delta q_2 + C_{11}C_{31}\delta q_3\right] \\ &\quad + K_1(\omega_3\delta\omega_2 + \omega_2\delta\omega_3) \\ \delta\dot{\omega}_2 &= K_2 6\Omega^2\left[C_{11}C_{21}\delta q_1 + \left(C_{31}^2 - C_{11}^2\right)\delta q_2 - C_{21}C_{31}\delta q_3\right] \\ &\quad + K_2(\omega_3\delta\omega_1 + \omega_1\delta\omega_3) \\ \delta\dot{\omega}_3 &= K_3 6\Omega^2\left[-C_{11}C_{31}\delta q_1 + C_{21}C_{31}\delta q_2 + \left(C_{11}^2 - C_{21}^2\right)\delta q_3\right] \\ &\quad + K_3(\omega_2\delta\omega_1 + \omega_1\delta\omega_2) \end{aligned} \tag{42}$$

IV. Results

The following section contains a compilation of attitude solutions and other results for RADCAL obtained with the methods described earlier. RADCAL is a symmetrical spacecraft in a near-circular, polar orbit at an altitude of 815 km, used by the U.S. Air Force for radar calibration. The physical parameters for RADCAL are given in Table 2. It is passively stabilized to a nadir pointing attitude by a gravity gradient boom and magnetic nutation dampers. RADCAL carries a heavily modified Trimble Navigation TANS Quadrex receiver, which measures the phase difference of GPS signals arriving at four microstrip patch antennas mounted on the zenith face of the vehicle.[14,17] Each antenna is canted outward 17.5 deg. The baseline coordinates given in Table 2 are expressed in the body reference frame defined in Eq. (33).

The phase differences between each of the three slaves and a master antenna are included in the telemetry stream and downloaded for postprocessing. In addition to the phase observation files, we also use the RADCAL navigation solutions corrected for selective availability by the U.S. Air Force using a method developed at the Applied Research Laboratories[23] and the precise GPS orbits calculated by the Jet Propulsion Laboratory.[24] A total of five data sets have been processed and analyzed, as listed in Table 3.

Attitude Initialization Results

A number of data sets have been processed and analyzed. The RADCAL data used to produce the results presented next were collected on day 160 of 1994 (9 June 1994). The data records start at noon and span almost 18 h. The a priori yaw, roll, and pitch for the attitude initialization were all chosen to be zero. The a priori values for the angular velocity and line biases were also set to zero. The baseline vectors were fixed to the values derived from the vehicle mechanical drawings. Using a 10-min span of data, the algorithm converged to an attitude solution in six iterations. The results are reported in Table 4. The fourth column reports the largest difference between line bias estimates $\Delta\beta$. For all data sets, the initialization attitude estimate was within 10 deg of the filter estimate.

Table 2 RADCAL parameters

	Parameter	Value
Nominal orbit[a]	Semimajor axis, km	7193
	Eccentricity	0.01
	Inclination, deg	90.0
Size[a]	Body height, cm	40.6
	Body diameter, cm	76.2
	Boom height, m	6.069
	Weight, kg	89.3
Moments[b]	Radial, kg m/s	6.234
	Transverse, kg m/s	96.242
	Normal, kg m/s	96.675
Baselines[b]	Baseline 1, m	[0.0 0.313 0.313]
	Baseline 2, m	[0.0 0.626 0.0]
	Baseline 3, m	[0.0 0.313 −0.313]

[a]Nominal orbit and size parameters taken from Ref. 18.
[b]Moments of inertia and baseline vectors taken from mechanical drawings.

Table 3 RADCAL data sets

Day	Date	Length, h	Data interval, s
079	20 March 94	2.2	15
107	17 April 95	5.9	12
160	9 June 94	17.6	30
165	14 June 94	11.2	30
189	8 July 94	16.8	30

Table 4 Attitude initialization results for RADCAL (day 160)

Euler angles, deg	Angular velocity, deg/s	Line biases, cycles	Line bias difference, cycles
Yaw: −164.1	ω_1: -8.0×10^{-4}	β_1: 0.72	$\Delta\beta_1$: 0.26
Roll: −3.0	ω_2: -4.4×10^{-4}	β_2: 0.44	$\Delta\beta_2$: 0.24
Pitch: 3.0	ω_3: 8.3×10^{-4}	β_3: 0.29	$\Delta\beta_3$: 0.22

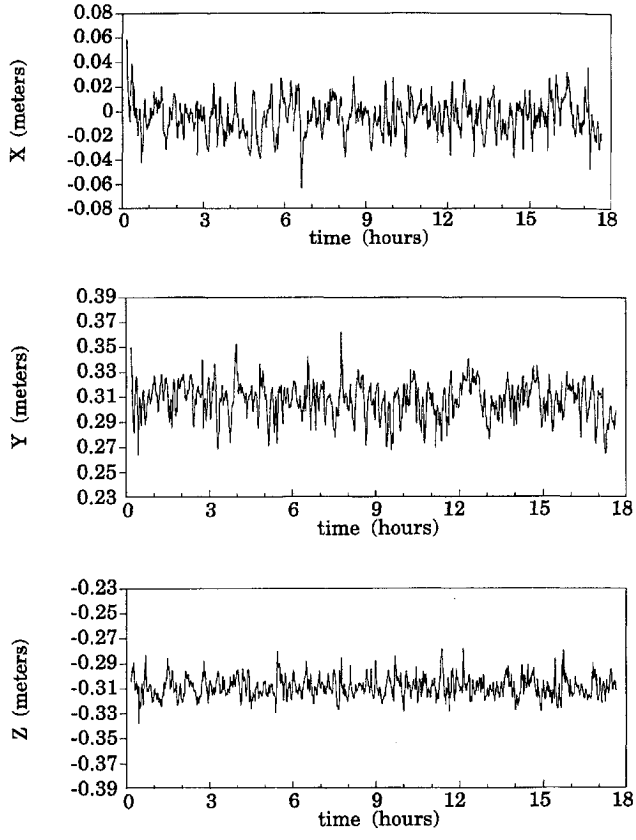

Fig. 5 Baseline 3 estimates in the body frame (day 160).

Since the quality of the RADCAL data is rather poor, finding a portion of data that would produce a consistent solution was not easy. On three of the data sets no interval met the minimum phase change per baseline requirement. On day 189 the length of the interval had to be increased as well. Occasionally, we also had to try more than one interval before finding one that produced a consistent solution. However, each time the line biases were consistent, the attitude solution was correct.

Baseline Estimation Results

The attitude and line biases from the initialization and baselines from the mechanical drawing provided the a priori values for the baseline estimator. The standard deviation of the measurement noise was set to 1 cm, and the process noise was chosen to allow for a 1-mm change in the baselines (expressed in local coordinates) over a 1-s interval. Phase difference measurements with an SNR of less than 3 AMU were eliminated from the solution. The estimates obtained on day 160 for baseline 3 are given in Fig. 5. Although the estimates are noisy, the trend remains constant, as expected. These results are typical of those obtained on other days as well. Table 5 contains the baseline estimation results for all days processed. The baselines from the mechanical drawings are also included. The estimates for each baseline coordinate are closely clustered. The maximum difference in baseline length between data sets is 7 mm. The largest angle between estimated baseline directions is 1 deg.

Attitude Kalman Filter Results

Baseline estimates and line biases from the baseline estimator and the attitude from the initialization routine provided the a priori values for the filter. The standard deviation of the measurement noise was set to 1 cm. The process noise over a 1-s interval was chosen to be $(1 \times 10^{-5})^2$ for the quaternion states, $(1 \times 10^{-6}$ rad/s$)^2$ for the angular velocity states, and $(1 \times 10^{-7}$ cycles$)^2$ for the line bias states.

The attitude estimates for day 160 are shown in Fig. 6. The quaternion estimates have been converted to Euler angles for presentation purposes. Although we cannot determine the actual filter error, the 1-σ uncertainties for day 160 reported by the Kalman filter are

Table 5 Baseline vector estimates

Day	Baseline 1, m			Baseline 2, m			Baseline 3, m			Line biases, cycles		
	b_x	b_y	b_z	b_x	b_y	b_z	b_x	b_y	b_z	β_1	β_2	β_3
079	0.0	0.310	0.304	0.0	0.618	0.0	−0.006	0.305	−0.308	0.888	0.484	0.163
107	0.0	0.306	0.311	0.0	0.615	0.0	−0.002	0.309	−0.310	0.894	0.477	0.165
160	0.0	0.303	0.308	0.0	0.614	0.0	−0.004	0.307	−0.309	0.893	0.502	0.173
165	0.0	0.306	0.307	0.0	0.620	0.0	−0.005	0.311	−0.312	0.922	0.499	0.163
189	0.0	0.304	0.309	0.0	0.621	0.0	−0.009	0.307	−0.309	0.900	0.468	0.164
Mech.	0.0	0.313	0.313	0.0	0.626	0.0	0.0	0.313	−0.313	—	—	—

Table 6 1-σ filter uncertainties

Day	Euler angle, deg	Angular velocity, arcsec/s	Line bias, cycle $\times 10^{-3}$
079	0.26	1.78	3.80
107	0.22	1.63	2.02
160	0.31	2.03	1.56
165	0.34	3.16	2.09
189	0.30	1.96	2.89

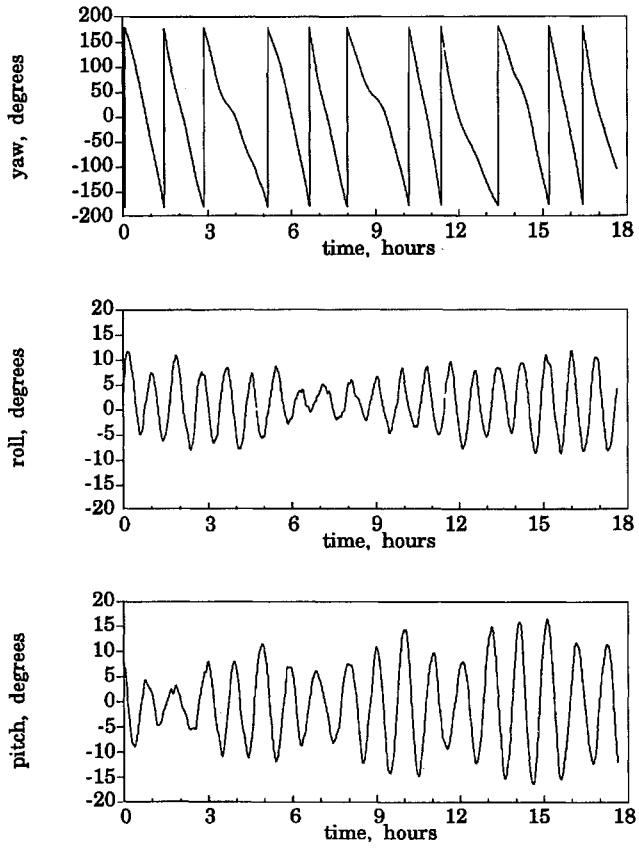

Fig. 6 Attitude filter solutions (day 160).

0.31 deg for the Euler angles, 2.0 arcsec/s for the angular velocities, and 1.6 mm for the line biases. The 1-σ uncertainties reported for all days are given in Table 6. Since the measurement noise is not white but structured as a result of multipath, and there is mismodeling in the filter, these bounds are probably optimistic.

In Fig. 6 we see that the spacecraft is slowly spinning about the yaw axis. The rate of spin is near the orbit rate but opposite in direction. Harmonic oscillations about the roll and pitch axes are also apparent, which is typical of gravity gradient motion. On days 079 and 107 the spacecraft displays similar behavior.

Results from day 189 shown in Fig. 7, however, indicated a different type of motion. The yaw angle is fairly constant for the first 4 h. The yaw rate then speeds up to the "normal" mode observed on RADCAL. Day 165 exhibits a similar period where the yaw is constant. Although the specific cause is not yet known, there must be different disturbing torques acting on the spacecraft during these periods. At this point we believe it is related to the magnetic dampers.

Table 7 RADCAL pitch and roll periods (in minutes)

Day	Roll period	Pitch period
Expected	52.47	60.85
107	54.01	64.80
160	52.94	62.30
165	51.84	61.28
189	49.54	60.57

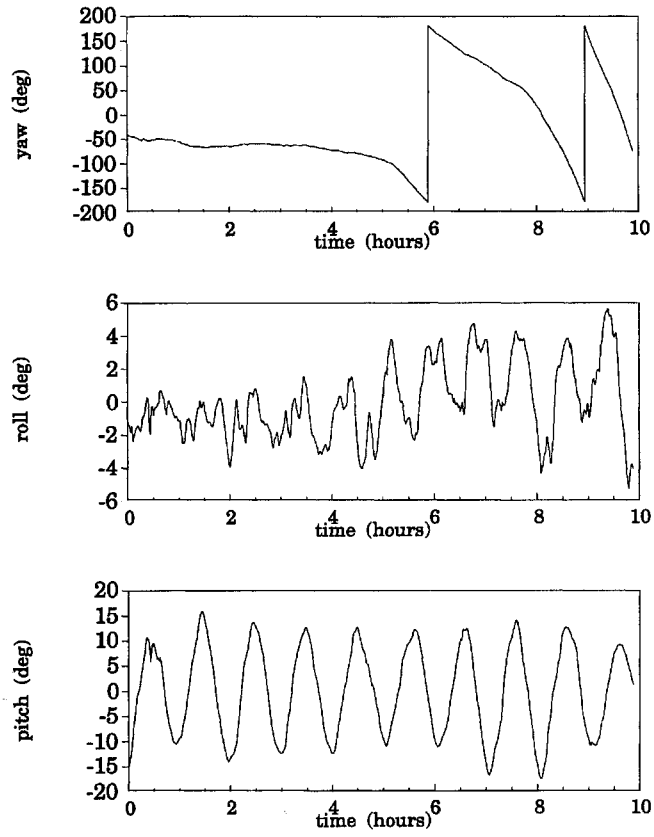

Fig. 7 Attitude filter solutions (day 189).

To further evaluate the results, we compared the expected and observed roll and pitch frequencies. The expected natural pitch and roll frequencies for a gravity gradient satellite can be calculated with the following equations[25]:

$$\omega_p = n\sqrt{3\frac{I_2 - I_1}{I_3}} \qquad \omega_r \approx n\sqrt{4\frac{I_3 - I_1}{I_2}} \tag{43}$$

The observed frequencies can be determined by taking a fast Fourier transform (FFT) of the RADCAL attitude solutions. From Fig. 8, which shows an FFT of the pitch angle estimates for day 160, it is clear that most of the power is concentrated at the natural frequency ($\sim 1.7 \times 10^{-3}$ rad/s), with very little power at the orbital frequency ($\sim 1.03 \times 10^{-3}$ rad/s). The FFT results for both pitch and roll are compiled in Table 7. The expected periods of the pitch and roll motions agree with the observed periods within 5.6 and 6.5%, respectively.

The FFT for day 189 also showed a strong secondary peak at 545 min. This is probably a result of the near-constant yaw angle

Table 8 Line bias filter results, cycles

Day	β_1	β_2	β_3
079	0.918	0.515	0.184
107	0.902	0.493	0.172
160	0.906	0.496	0.180
165	0.910	0.493	0.179
189	0.900	0.494	0.180

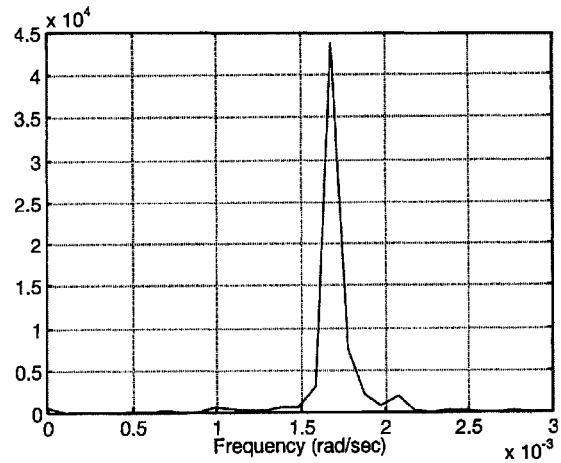

Fig. 8 FFT of pitch angle (day 160).

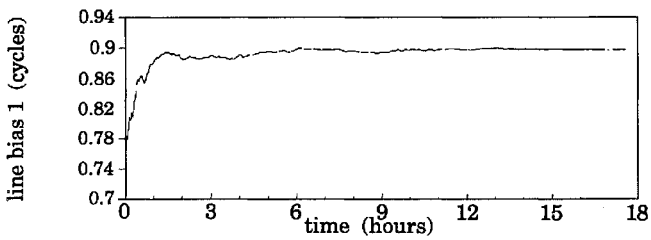

Fig. 9 Line bias 1 filter solutions (day 160).

observed at the beginning of the data set. The data for day 079 spanned less than two orbital periods and, hence, the data interval was too short to produce meaningful results.

Line bias consistency is yet another indication of filter performance. Figure 9 shows the solutions for line bias 1 on day 160. Although it takes an hour to converge, the estimates remain constant for the remainder of the run, as expected. The standard deviation of the estimates, excluding the first hour of data, is 0.02 cycles (4 mm). These results are characteristic of line bias solutions obtained not only on other baselines but on other days as well. Line bias estimates in cycles for all days are compiled in Table 8. There is strong agreement in line bias estimates across each day. The largest difference of 4.4 mm occurs on line bias 2.

In addition to looking at attitude solutions, we looked at measurement residuals from the filter to gain insight on its performance. In many cases the residuals were structured with a time constant corresponding to multipath reflections from the boom. Although the antennas were canted outward to decrease multipath from the boom, the results are clearly corrupted by multipath. Furthermore, although the canting increases the total sky visibility, it decreases the number of satellites in common view. In addition, phase center motion will generally cancel out if all of the antennas are pointed in the same direction; however, canting the antennas is likely to introduce an additional error as a result of phase center motion.

Attitude Point Solution Results

For comparison, we also processed the data with the least-squares point solution. Again, the attitude from the initialization algorithm was used to start the process. The line biases were fixed to the estimates calculated in the attitude Kalman filter. Measurements with SNRs of less than 3 AMU were excluded from the solution. Although the point solutions are noisier than the filter solutions, they

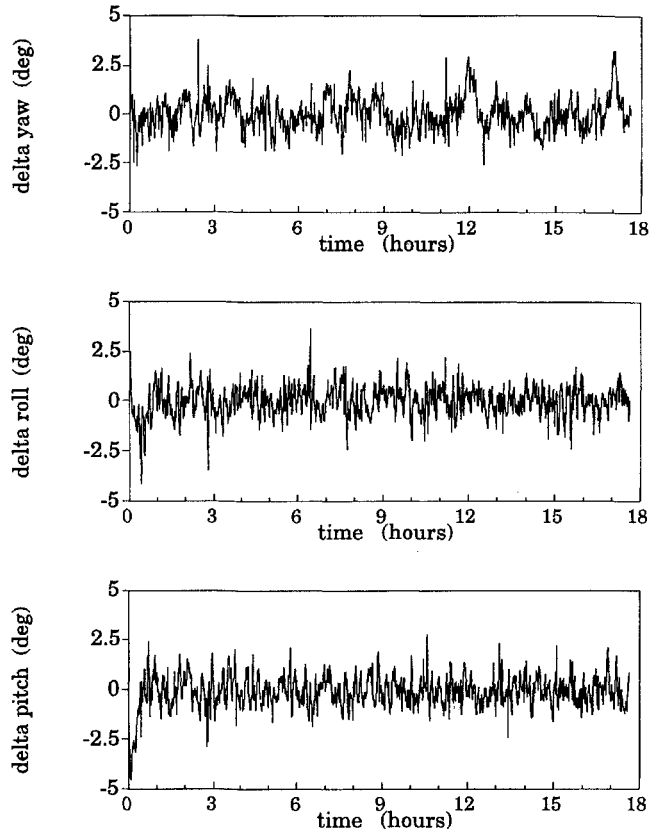

Fig. 10 Point vs filter attitude difference (day 160).

are qualitatively similar. The attitude difference formed by subtracting the point solutions from the filter solutions for day 160 is plotted in Fig. 10.

The differences shown in Fig. 10 represent the combination of both point and filter errors where errors common to both solution methods have canceled out. The point solutions track the measurement data, so point solution errors are likely to be dominated by errors in the GPS measurements, which include receiver noise and multipath. One other potential source of error would be inaccuracies in the baseline estimates; however, these are common to the filter solution and cancel out when comparing the two methods. Because each GPS satellite pass is fairly short (~20 min), there is no viable mechanism for low-frequency errors to appear in the point solutions.

The filter solution has removed or smoothed the measurement errors by establishing a fairly high confidence in the dynamic model; i.e., by setting the process noise values low. Filter solution errors are caused by dynamic mismodeling and are evident in the lower-frequency components of the solution differences. In particular, we expect to see the effects of unmodeled disturbances in the range of once or twice the orbital rate.

To investigate this we first performed an FFT of the difference data. This produced several low-frequency power spikes in the range of one cycle per 50–100 min, in particular at once and twice the orbital rate. These are clearly a result of dynamic mismodeling in the filter. There was also power at higher frequencies of one cycle per 5–10 min, which is likely a result of multipath, and additional power in the one cycle per 10–20 min range, which may be caused by low-frequency multipath and/or high-frequency dynamic effects.

To quantify the contributions in each frequency regime, we computed the rms values of the raw difference data and compared them with the rms values of low pass filtered (LPF) versions of the same data. The results are given in Table 9. The rms of the unfiltered difference is probably indicative of the point solution accuracy, which is approximately 0.8 deg per axis.

Using a Butterworth filter, we set the first low pass filter cutoff frequency at one cycle per 10 min to eliminate errors that are clearly a result of measurement noise. This produced an rms of about 0.5 deg in the pitch and roll axes and as much as 0.7 deg in the yaw axis. The larger result in the yaw axis indicates that there are likely to

Table 9 Point and filter solution difference rms in degrees

Day	Angle	Raw	10-min LPF	20-min LPF
160	Yaw	0.82	0.71	0.66
	Roll	0.63	0.44	0.29
	Pitch	0.63	0.47	0.31
189	Yaw	0.58	0.42	0.34
	Roll	0.73	0.55	0.38
	Pitch	0.62	0.47	0.32

be significant unmodeled disturbance torques in this direction. Note that on day 189 when the yaw was constant for a long interval, the results were improved. This indicates that under these conditions there was probably a lower level of yaw disturbance torque acting on the spacecraft.

To investigate the performance of the filter assuming that the errors in the one cycle per 10–20 min range are also measurement errors, we then set the cutoff frequency to one cycle per 20 min. The resulting rms values were reduced to less than 0.4 deg per axis in pitch and roll angles. To further investigate the filter mismodeling and get a better understanding of its performance it would be necessary to augment the dynamic model as described in the following section.

V. Summary and Future Work

This paper describes a sequence of algorithms for GPS-based attitude estimation of a near-Earth gravity gradient satellite. Each algorithm represents increasing requirements for a priori knowledge of the vehicle state and dynamics, which consequently improves output accuracies. The algorithms have all been successfully applied to actual flight data collected on board the U.S. Air Force RADCAL satellite, and the results have been presented.

Under the current implementation, baselines and attitude can both be determined but not simultaneously. By combining the two steps, however, the attitude estimation process could be simplified and streamlined. The approach under investigation is to estimate a reduced set of baseline parameters along with the attitude quaternion. Since the baselines would not necessarily be fixed, this algorithm would have potential application for spacecraft with GPS antennas mounted on flexible appendages or for very large spacecraft such as the NASA Space Station.

We also plan to investigate how unmodeled torques affect the accuracy of the attitude filter. This will include identifying significant perturbations, quantifying their effects of vehicle attitude, and determining which perturbations, if any, should be added to the attitude filter dynamics to obtain the required performance.

Acknowledgments

This research was sponsored by the U.S. Naval Research Laboratory under Grant N00014-93-1-G030 and by the Patricia Roberts Harris Foundation. The authors would like to acknowledge the assistance of Bill Feess, Robert Smith, and Tom Alley of The Aerospace Corporation in providing us access to the RADCAL data files and mechanical drawings. We would also like to thank Clark Cohen and Glenn Lightsey of Stanford University for providing much useful information about the operation of the GPS receiver on board RADCAL.

References

[1]Shuster, M., "Survey of Attitude Representations," *Journal of the Astronautical Sciences*, Vol. 41, No. 4, 1993, pp. 439–517.

[2]Lefferts, E. G., Markley, F. L., and Shuster, M. D., "Kalman Filtering for Spacecraft Attitude Estimation," *Journal of Guidance, Control, and Dynamics*, Vol. 5, No. 5, 1982, pp. 417–429.

[3]Markley, F. L., "Attitude Determination Using Vector Observations and the Singular Value Decomposition," *Journal of the Astronautical Sciences*, Vol. 36, No. 3, 1988, pp. 245–258.

[4]Shuster, M. D., and Oh, S. D., "Three-Axis Attitude Determination from Vector Observations," *Journal of Guidance and Control*, Vol. 4, No. 1, 1981, pp. 70–77.

[5]Wertz, J. R. (ed.), *Spacecraft Attitude Determination and Control*, Kluwer, Dordrecht, The Netherlands, 1978.

[6]Chesley, B. C., "An Integrated GPS Attitude Determination System for Small Satellites," Ph.D. Dissertation, Dept. of Aerospace Engineering Sciences, Univ. of Colorado, Boulder, CO, 1995.

[7]Satz, H. S., Cox, D. B., Beard, R. L., and Landis, G. P., "GPS Inertial Attitude Estimation via Carrier Accumulated-Phase Measurements," *Navigation*, Vol. 38, No. 3, 1991, pp. 273–284.

[8]Melvin, P., "A Kalman Filter for a Gravity Gradient Satellite," *Advances in the Astronautical Sciences*, Vol. 76, 1991, pp. 763–782.

[9]Albertine, J. R., "An Azimuth Determination System Utilizing the Navy Navigation Satellites," *Navigation*, Vol. 21, No. 1, 1974, pp. 54–60.

[10]Rath, J., and Ward, P., "Attitude Estimation Using GPS," *Proceedings of the ION National Technical Meeting* (San Mateo, CA), Inst. of Navigation, Alexandria, VA, 1989, pp. 169–178.

[11]Brown, A. K., Bowles, W. M., and Thorvaldsen, T. P., "Interferometric Attitude Determination Using the Global Positioning System: A New Gyrotheodolite," *Proceedings of the 3rd International Geodetic Symposium in Satellite Doppler Positioning* (Las Cruces, NM), 1982, pp. 1289–1302.

[12]Van Graas, F., and Braasch, M., "GPS Interferometric Attitude and Heading Determination: Initial Flight Test Results," *Navigation*, Vol. 38, No. 4, 1991–1992, pp. 297–317.

[13]Lu, G., Cannon, M. E., and Lachapelle, G., "Attitude Determination in a Survey Launch Using Multi-Antenna GPS Technologies," *Proceedings of the ION National Technical Meeting* (San Francisco, CA), Inst. of Navigation, Alexandria, VA, 1993, pp. 251–259.

[14]Anon., "TANS Vector Specification and User's Manual," Trimble Navigation, Ltd., Sunnyvale, CA, May 1994.

[15]Cohen, C. E., "Attitude Determination Using GPS," Ph.D. Dissertation, Dept. of Aeronautics and Astronautics, Stanford Univ., Standard, CA, Dec. 1992.

[16]Cohen, C. E., "Attitude Determination," *Global Positioning System: Theory and Applications, Volume II*, edited by B. W. Parkinson and J. J. Spilker, Vol. 164, Progress in Astronautics and Aeronautics, AIAA, Washington, DC, 1996, pp. 519–538.

[17]Lightsey, E. G., Cohen, C. E., and Parkinson, B. W., "Application of GPS Attitude Determination to Gravity Gradient Stabilized Spacecraft," *Proceedings of the AIAA Guidance, Navigation, and Control Conference* (Monterey, CA), TP, Pt. 2, AIAA, Washington, DC, 1993, pp. 820–826.

[18]Lightsey, E. G., Cohen, C. E., Fees, W. A., and Parkinson, B. W., "Analysis of Spacecraft Attitude Measurements Using Onboard GPS," *Advances in the Astronautical Sciences*, Vol. 86, 1994, pp. 521–532 (AAS 94-063).

[19]Cohen, C. E., Lightsey, E. G., Parkinson, B. W., and Feess, W. A., "Space Flight Tests of Attitude Determination Using GPS," *International Journal of Satellite Communications*, Vol. 12, 1994, pp. 427–433.

[20]Cohen, C. E., and Parkinson, B. W., "Integer Ambiguity Resolution of the GPS Carrier for Spacecraft Attitude Determination," *Advances in the Astronautical Sciences*, Vol. 78, 1992, pp. 107–118 (AAS Paper 92-015).

[21]Axelrad, P., and Ward, L. M., "On-Orbit GPS Based Attitude and Antenna Baseline Estimation," *Proceedings of the ION National Technical Meeting* (San Diego, CA), Inst. of Navigation, Alexandria, VA, 1994, pp. 441–450.

[22]Kane, T. R., Likins, P. W., and Levinson, D. A., *Spacecraft Dynamics*, McGraw-Hill, New York, 1983.

[23]Langer, J. V., Feess, W. A., Harrington, K. M., Bacigalupi, M. R., Cardoza, M. A., Mach, R. G., and Abusali, P. A. M., "RADCAL: Precision Orbit Determination with a Commercial Grade GPS Receiver," *Proceedings of the ION National Meeting* (San Diego, CA), Inst. of Navigation, Alexandria, VA, 1994, pp. 421–431.

[24]Zumberge, J. F., and Bertiger, W. I., *Global Positioning System: Theory and Applications, Volume I*, edited by B. W. Parkinson and J. J. Spilker, Vol. 163, Progress in Astronautics and Aeronautics, AIAA, Washington, DC, 1996, pp. 585–599.

[25]Chobotov, V. A., *Spacecraft Attitude Dynamics and Control*, Krieger, Malabar, FL, 1991.